Published in IEEE Transactions on Electromagnetic Compatibility,
Volume: 59, Issue: 1, pp. 111- 118, Feb. 2017

A Modular Test-Suite for the Validation and Verification of Electromagnetic Solvers in Electromagnetic Compatibility Applications

Ian D. Flintoft, *Senior Member, IEEE*, John F. Dawson, *Member, IEEE*, Linda Dawson, Andrew C. Marvin, *Fellow, IEEE*, Jesus Alvarez, *Member, IEEE*, and Salvador G. Garcia, *Senior Member, IEEE*

***Abstract*—Computational solvers are increasingly used to solve complex electromagnetic compatibility (EMC) problems in research, product design, and manufacturing. The reliability of these simulation tools must be demonstrated in order to give confidence in their results. Standards prescribe a range of techniques for the validation, verification, and calibration of computational electromagnetics solvers including external references based on measurement or for cross-validation with other models. We have developed a modular test-suite based on an enclosure to provide the EMC community with a complex external reference for model validation. We show how the test-suite can be used to validate a range of electromagnetic solvers. The emphasis of the test-suite is on the features of interest for EMC applications, such as apertures and coupling to cables. We have fabricated a hardware implementation of many of the test-cases and measured them in an anechoic chamber over the frequency range to 1–6 GHz to provide a measurement reference for validation over this range. The test-suite has already been used extensively in two major aeronautical research programs and is openly available for use and future development by the community.**

***Index Terms*—Benchmark problems, computational electromagnetics (CEM), validation, verification.**

I. Introduction

TO ENABLE the use of computational electromagnetics (CEM) for both research and certification purposes, it is necessary to prove the reliability of the computational modeling at producing realistic results. For this, it is necessary to apply a systematic validation, verification, and calibration (VV&C) process for the development and deployment of CEM tools. A detailed explanation of the different aspects of VV&C in the context of CEM and electromagnetic compatibility (EMC) is provided in [1]. In brief, the three keys terms are defined by Oberkampf *et al.* [2] and Trucano and Hirsch [3]:

1) Validation: "The process of determining the degree to which a model is an accurate representation of the real world from the perspective of the intended uses of the model."
2) Verification: "The process of determining that a model implementation accurately represents the developer's conceptual description of the model and the solution to the model."
3) Calibration: "The process of adjusting numerical or physical modeling parameters in the computational model for the purpose of improving agreement with experimental data."

VV&C relies in part on the application of well-defined canonical or benchmark reference problems [4]. Often these reference cases are based on exact analytical results for very simple geometries, though measurement references can also be used. Example reference models suitable for VV&C of CEM tools can be found in [4] and [5]. Such reference cases can also be used for cross-validation between different CEM solvers, which is particularly salient to more complex reference problems for which analytic solutions are not available. Indeed, it is for the VV&C of complex structures that involve the interaction of many different submodels within an overall simulation where there is a need for more systematic reference cases backed by reliable measurement.

In this paper, we describe a modular test-suite of intermediate complexity that has been used extensively within two major research projects for the validation of CEM codes, with an emphasis on EMC applications. The test-suite geometry is designed to cover a wide range of frequencies and operating modes, from quasi-static to reverberant. It allows comparison of the different features and the capabilities of various solvers to describe these features, for example, apertures, materials, and wires. A hardware implementation of the test object has been fabricated along with all of the modular components to allow measurement validation data to be obtained.

The test-suite is based on a hardware object that was originally constructed for the validation of a hybrid finite-difference time-domain/finite element solver for aerospace simulations [6], [7]. The geometry was used again and extended as a numerical test-suite for the development of a computational simulation framework for certification of aircraft against high intensity radio-frequency (HIRF) threats [8], [9]. Further development

Manuscript received March 31, 2016; revised July 22, 2016; accepted July 31, 2016. Date of publication August 29, 2016; date of current version October 25, 2016. This work was supported by the U.K. Engineering and Physical Sciences Research Council under the Flapless Air Vehicle Integrated Industrial Research program under Grant GR/S71552/01, and from the European Community's Seventh Framework Program FP7/2007-2013 under Grant 205294 on the High Intensity Radio-frequency Field Synthetic Environment research project.

I. D. Flintoft, J. F. Dawson, L. Dawson, and A. C. Marvin are with the Department of Electronics, University of York, Heslington, York YO10 5DD, U.K. (e-mail: ian.flintoft@york.ac.uk; john.dawson@york.ac.uk; l.dawson@york.ac.uk; andy.marvin@york.ac.uk).

J. Alvarez is with the Airbus Defence and Space, 28906 Getafe, Spain (e-mail: jesus.g.alvarez@airbus.com).

S. G. Garcia is with the Department of Electromagnetism and Matter Physics, University of Granada, 18071 Granada, Spain (e-mail: salva@ugr.es).

Color versions of one or more of the figures in this paper are available online at http://ieeexplore.ieee.org.

Digital Object Identifier 10.1109/TEMC.2016.2599004

work continues for application in high-frequency shielding simulations [10].

The rationale for the test-suite was to construct a rigorously controlled and characterized generic object that incorporated features of interest to the EMC community, such as:

1) Coupling through apertures and joints.
2) Coupling to transmission lines.
3) Low loss, high Q-factor enclosures.
4) Absorption of radio-frequency energy by absorbing materials.

These features were designed in a modular fashion, allowing for the validation of single elements (for example, an aperture model) or a combination of elements. It was also an objective to construct a hardware implementation of the test object that was suitable for accurate measurements up to 6 GHz. The final outcome was a test object consisting of a metallic box with a number of tests ports and an interchangeable panel that could contain apertures and joints and a selection of internal components such as wires and absorbers. It also includes a number of elements which act as transmission lines with varying levels of complexity (single straight wire, curved wire and a multiple conductor, straight transmission line).

The test-suite is described in detail in Section II. The measurements used to characterize the probe antennas and collect reference data for a selection of the test-cases are presented in Section III. In Section IV, summary results of simulations of a small subset of the tests-cases in the frequency range 1–6 GHz using a range of solvers are presented and compared using feature selective validation (FSV), taking the measurement data as a reference. We conclude in Section V.

II. Test-Object Description

A. Enclosure

The test object is based on a physical brass box of (internal) dimensions 600 mm × 500 mm × 300 mm with a removable "front" face. The thickness of the walls is 1 mm to ensure that all energy penetration is due to the apertures. The physical geometry of the box is shown in Fig. 1. The front face can be left open or covered with a plate with different characteristics. The open face has a 30-mm-wide flange around the edge with holes spaced at 26 mm (sides) and 28 mm (top and bottom) for fixing the interchangeable covering plates using 60 stainless steel captive bolts that protrude outwards. The box has three N-type connectors on the top, labeled A, B, and C in the figure. Probe antennas or wire structures can be connected to these three ports. Additionally, absorbing material or other structures can be placed in the volume of the enclosure. A photograph of the enclosure is shown in Fig. 2.

The lowest cavity mode in the empty enclosure, with the front face closed, is at 390 MHz. At 1 GHz there are a total of 44 propagating modes and by 2 GHz this rises to around 300. The mode density at 2 GHz is 0.48 MHz^{-1} rising to 3.2 MHz^{-1} at 6 GHz. As a reverberation chamber the lowest usable frequency of the enclosure is approximately 1.5 GHz [11]. The frequency range therefore includes the physically interesting intermediate frequency range in which full-wave solvers begin to require prohibitive computational resources when applied to large objects such as complete aircraft and asymptotic solvers are still of limited validity.

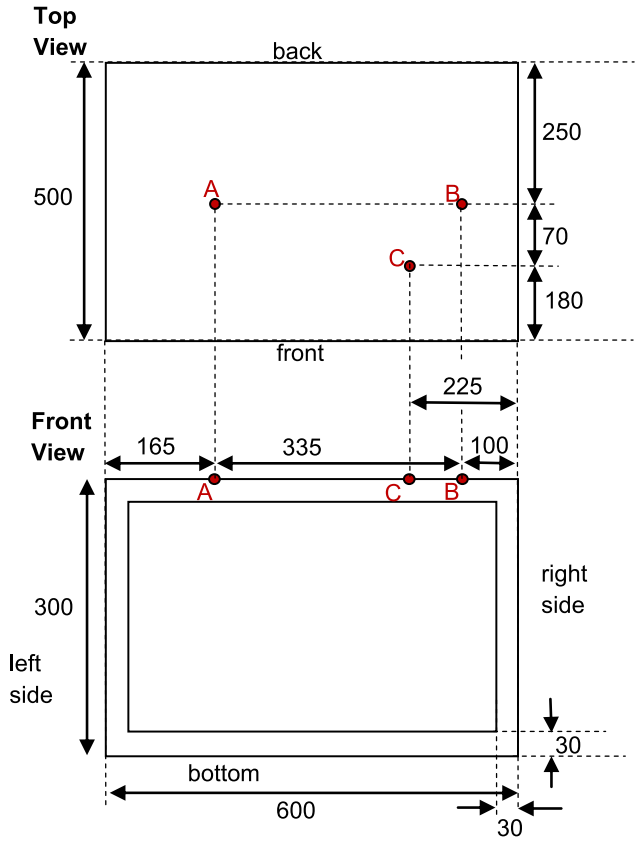

Fig. 1. Physical dimensions (in millimeters) of the test-object enclosure.

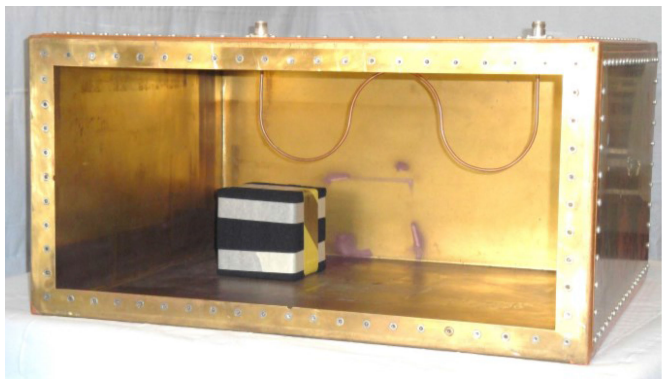

Fig. 2. Photograph of the physical test-object enclosure.

B. Monopole Probes

Monopole probes can be attached to ports A, B, or C. The physical probes are constructed using 50 Ω N-Type bulkhead connectors and 3-mm-diameter brass rod. The overall length of the monopoles from the internal side of the wall to the tip is 22 mm.

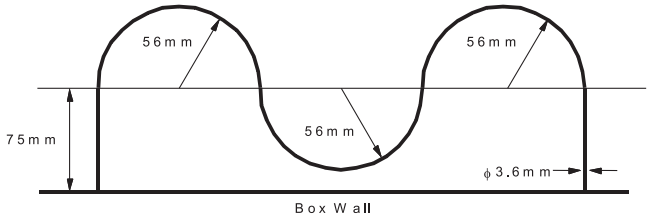

Fig. 3. Geometry of the curved wire that can be attached between port-A and port-B.

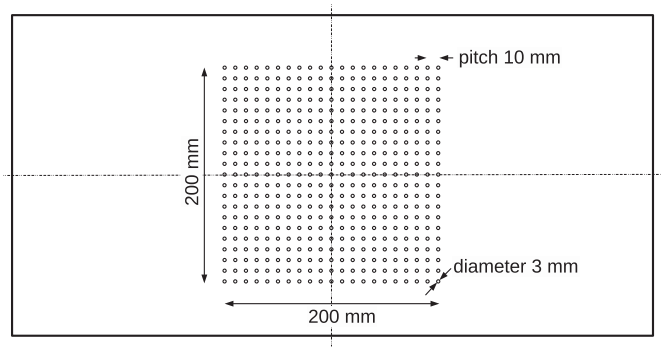

Fig. 4. Dimensions of the perforated plate front panel consisting of an array of circular holes arranged in a square grid.

C. Wires and Looms

A straight wire made from 3.5-mm-diameter brass rod can be soldered to the ends of two probe antennas attached to ports A and B, thus forming a uniform transmission line of height 22 mm and length 335 mm. In addition, a curved wire has been fabricated, as shown in Fig. 3. This can also be soldered to the probes in the same ports. A more complex but well-defined loom consisting of six 1-mm-diameter wires arranged in a hexagonal cross section has also been defined in the full test-suite [16].

D. Apertures, Grills, and Joints

The enclosure can be used with an open face or a completely closed face. The physical implementation of the test-object with a fully closed face has been measured to have an isolation factor between the inside and outside of more than 90 dB up to 6 GHz. It is ultimately limited by the clamping pressure of the machine screws used to hold it in place and the surface finish of the brass plates. Care must be taken to ensure that the clamping pressure is consistent, particularly when the apertures in the face are not significantly larger than the spacing between the screws. Above 6 GHz, the separation of the fasteners is more than half a wavelength and the isolation degrades.

Further possibilities for the covering plate include aperture and joints structures. Fig. 4 shows a perforated plate consisting of an array of 3-mm-diameter circular holes arranged on a 21×21 square grid with a pitch of 10 mm. The plate thickness is 0.3 mm and the hole array is centered on the panel face. Regarded as an infinite array, the shielding effectiveness (SE) of the array exhibits a 20 dB/decade increase with frequency until approximately 7 GHz where the electrical size of the holes is approximately one-tenth of a wavelength.

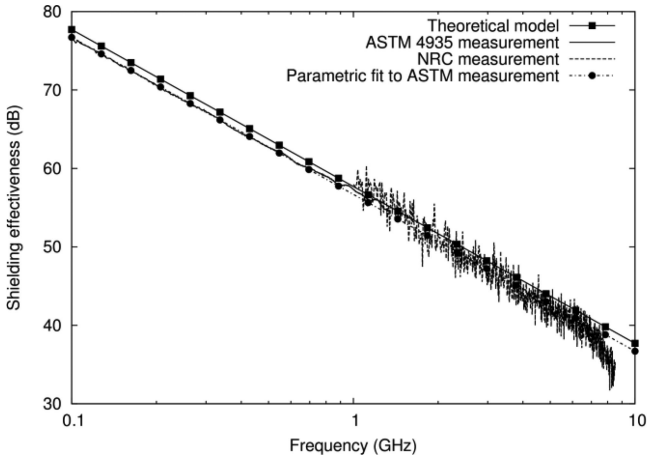

Fig. 5. Plane wave SE of an infinite perforated plate with the same characteristics as the front plate.

An approximate theoretical prediction for the normal incidence plane-wave SE of an infinite plate uniformly perforated with circular holes of radius a and pitch Δ is given by

$$\text{SE (dB)} = 20\log_{10}\frac{3c_0\Delta^2}{16\pi a^3} - 20\log_{10} f\,(\text{MHz}) - 32\frac{t}{2a} - 120 \quad (1)$$

where t is the plate thickness and c_0 is the speed of light in free-space [12] . This prediction is based on Bethe's small aperture polarizability theory and neglects the mutual coupling between the apertures. The penultimate term is added phenomenologically to account for the attenuation due to the cut-off waveguide effect of the sample thickness. For the above plate dimensions, the contribution of the finite thickness term is 3.2 dB.

The physical implementation of the perforated plate was measured in an ASTM4935 coaxial cell [13] and nested reverberation chambers (NRCs) [14]; the results are shown in Fig. 5 compared to the theoretical model. The measurement using the NRCs exhibits a statistical variation of about 4 dB due to the limited number of independent samples (32) taken in the measurement. A parametric fit to the measurement data gives

$$\text{SE (dB)} = 116.7 - 20\log_{10} f\ (\text{MHz}) \quad (2)$$

which is within 1 dB of the above model. A two-sided surface impedance boundary condition corresponding to a shunt inductance of 42 pH provides a good model of the perforated plate over the frequency range from 1 MHz to 6 GHz [15]. Other similar perforated plates have also been defined for use with the test object including anisotropic cases with rectangular slots at various angles with respect to the plate axes [16].

Front panels with larger apertures have also been defined and constructed. Fig. 6 shows a generic panel with two large apertures. The square aperture has a side length of 180 mm and the circular aperture diameter of 100 mm. The physical implementation uses a 0.3-mm-thick brass plate. These large apertures are useful for reducing the quality factor of the enclosure and increasing the energy coupled into the enclosure.

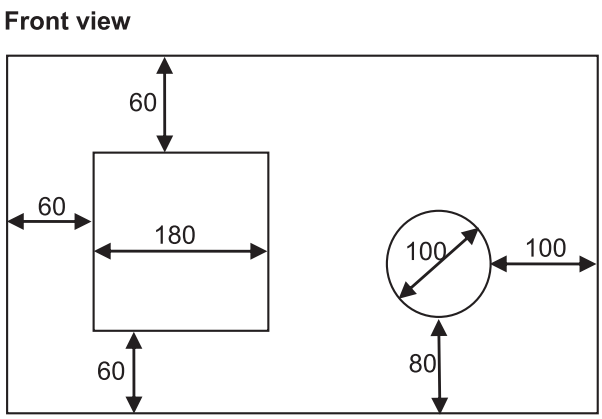

Fig. 6. Generic front plate with two large apertures. All dimensions are in millimeters.

TABLE I
DEBYE PARAMETERS OF LS22 RAM DETERMINED FROM A VECTOR FIT TO THE MANUFACTURER'S COMPLEX PERMITTIVITY DATA ($\varepsilon_\infty = 1$)

Parameter	$i = 1$	$i = 2$	$i = 3$
$\Delta\varepsilon_i\,(-)$	3.31	4.43	25.1
$\tau_i\,(\mathrm{ps})$	13.0	116	443

E. Internal Absorbers

The enclosure is a high quality factor environment. Even with the front face left completely open there exist "end-to-end" modes with Q-factors in the low thousands over the frequency range from 1 to 6 GHz. It is therefore often necessary or useful to damp the resonant behavior by introducing an absorber into the enclosure. The absorbing object itself can also be used to validate material models in computational tools.

The simplest absorbing element is a cubic piece of radio absorbing material (RAM) with a side length of 110 mm. The physical implementation was constructed from a number of layers of commercially available Eccosorb LS22 Series RAM sheet. The material is characterized by the manufacturer from 500 MHz to 18 GHz using the real and imaginary parts of the complex relative permittivity [17]. These material parameters have been fitted to a third-order Debye relaxation model

$$\varepsilon_r\,(s) = \varepsilon_\infty + \sum_{i=1}^{3} \frac{\Delta\varepsilon_i}{1 + s\tau_i} \tag{3}$$

using a vector fitting algorithm [18]. Here, we require that $\varepsilon_\infty \geq 1$ for stability for the model. The parameters of the Debye model are given in Table I, where in this case we have enforced $\varepsilon_\infty = 1$. The Debye model and manufacturer's data are compared in Fig. 7.

The fit is accurate within the expected experimental uncertainty in the manufacturer's measurement data and production tolerances over the frequency range from 1 to 6 GHz. Better fits can be obtained by allowing ε_∞ to vary or by including an ionic conductivity term $-\sigma_i/j\omega\varepsilon_0$ in the model, however, such models are not widely supported in computational solvers.

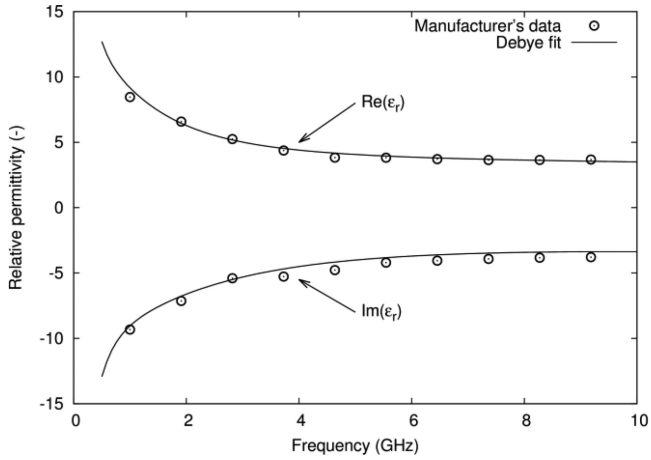

Fig. 7. Complex permittivity of LS22 absorber, comparing the manufacturer's data with a third order Debye model.

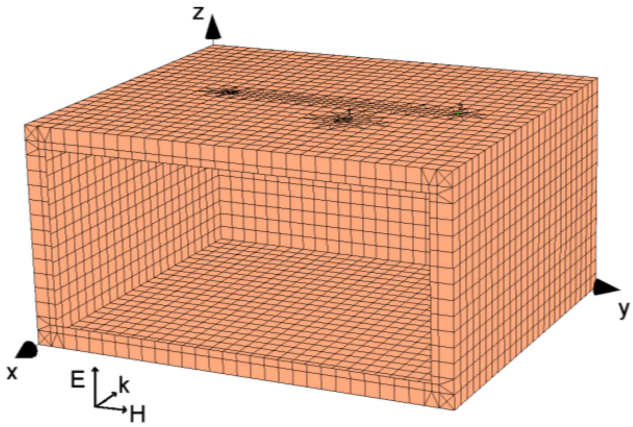

Fig. 8. Orientation of the unit plane wave excitation with vertical polarization (lower left) depicted on a computational mesh of the enclosure with an open face (CONCEPT-II mesh [20]).

F. Source Parameters and Observables

Two types of excitation have been defined for the test configurations: port excitation and external plane wave illumination. For port excitation, a matched source is used to inject power into port-A, which is connected to either a probe or wire. Such excitations are useful for detailed and accurate analysis of the behavior of the internal fields and surfaces currents.

For EMC immunity assessment, external illumination is of interest and so two plane wave sources are defined. First, a unit plane wave source consisting of a single monochromatic, linearly polarized plane wave of amplitude 1 V/m illuminating the front face of the box as shown in Fig. 8. Both vertical (z-direction) and horizontal (y-direction) polarizations of the electric field are considered. A multiple plane wave source was also defined to take into account several plane waves illuminating the enclosure in order to validate the computation of short-circuited electromagnetic fields on apertures by asymptotic codes or full-wave codes for simulation scenarios of numerical coupling between external and internal solvers.

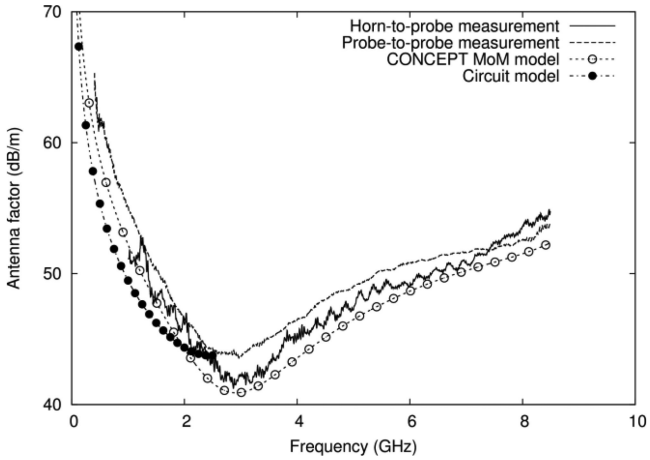

Fig. 9. Antenna factor of the probe antennas, comparing measurement results, MoM simulation and a circuit model.

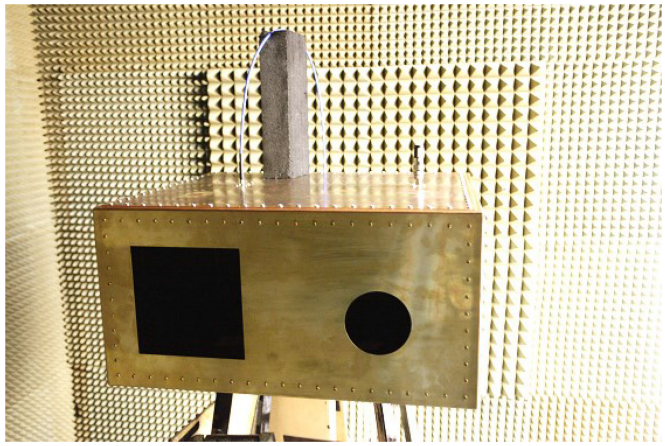

Fig. 10. Test-case with generic front plate on-test in an anechoic chamber.

Three types of observable are defined for the test-cases:

1) Power in a 50 Ω load connected to a port.
2) Power density inside the cavity.
3) Electric field strength at the centers of apertures.

In this paper, we only consider the first of these; the power received in a load connected to one of the probes, P_{rec}. For internal port sources, the observables are usually presented as scattering parameters between the ports while for external illumination the received power is typically normalized to the incident power density at the front face of the enclosure S_{inc} to give a reception aperture

$$A_{\mathrm{rec}} = P_{\mathrm{rec}}/S_{\mathrm{inc}}. \tag{4}$$

III. Measurement of Hardware Configurations

A. Probe Characterization

The hardware monopole probes have been calibrated by determining their free-space antenna factor (AF). This also allows the electric field strength from a simulation to be compared directly to the measurement data without the use of a wire model for the probe. This calibration was carried out using one-antenna and two-antenna methods [19], supported by boundary element method-of-moments (MoM) simulations and a circuit model. The results are shown in Fig. 9.

For the two-antenna method, a reference ridged-waveguide horn antenna was used to measure the AF of each probe over a ground plane in the frequency range 1–8.5 GHz, the lower limit been determined by the working range of the horn. This showed that the two probes were almost identical in terms of their AFs (less than 0.2 dB difference); therefore only one of these measurement results is shown in Fig. 9. This measurement configuration is however subject to uncertainty due to diffraction effects when trying to launch a uniform plane-wave above the ground plane. A one-antenna method was therefore also applied over the band 200 MHz–8.6 GHz, measuring the transmission between the two probes placed a known distance apart over an extended ground plane located in an anechoic environment. The fields in this configuration are subject to less uncertainty; the corresponding AF in Fig. 9 is typically a few decibels higher than the horn measurement.

The figure also shows the results of a MoM simulation of a probe above an infinite ideal ground-plane [20] and a simple circuit model of the monopole [21]. The MoM simulation used a thin-wire model of the monopole, which will introduce an error due to the relatively large diameter of the monopoles. The simple circuit model stops at 2 GHz as this model is only valid to just beyond the first resonance of the monopoles. These results indicated the typical uncertainty that may be encountered when comparing measurement and simulation made under different assumptions and approximations.

To determine the phase delay between the reference plane of the probe connector and the base of the monopole, the probe was shorted to the ground plane using metal foil and the complex reflection coefficient was measured relative to the reference plane. Calibration of this phase delay is important when comparing the measurement results to simulation data at high frequencies.

B. Anechoic Chamber Measurements

Most of the measurements on hardware configurations took place in an anechoic chamber over a frequency range 1–6 GHz using a vector network analyzer with cable effects and the phase delay of antennas calibrated out. Fig. 10 is a photograph of the enclosure with the front panel with two large apertures in place being tested in an anechoic room. The enclosure was illuminated by a horn antenna located near the camera position to generate a plane-wave source condition. The power received at port-A is being monitored by the blue test cable while the other port is terminated. To calibrate the incident power density, the enclosure was removed and another co-polar horn placed with its phase center at the location of the front face.

IV. Selected Results

In this section, we report simulation results from a number of the test-cases implemented using a range of solvers. The implementations were made directly from the written test-case specification, so for example, no computer aided design (CAD)

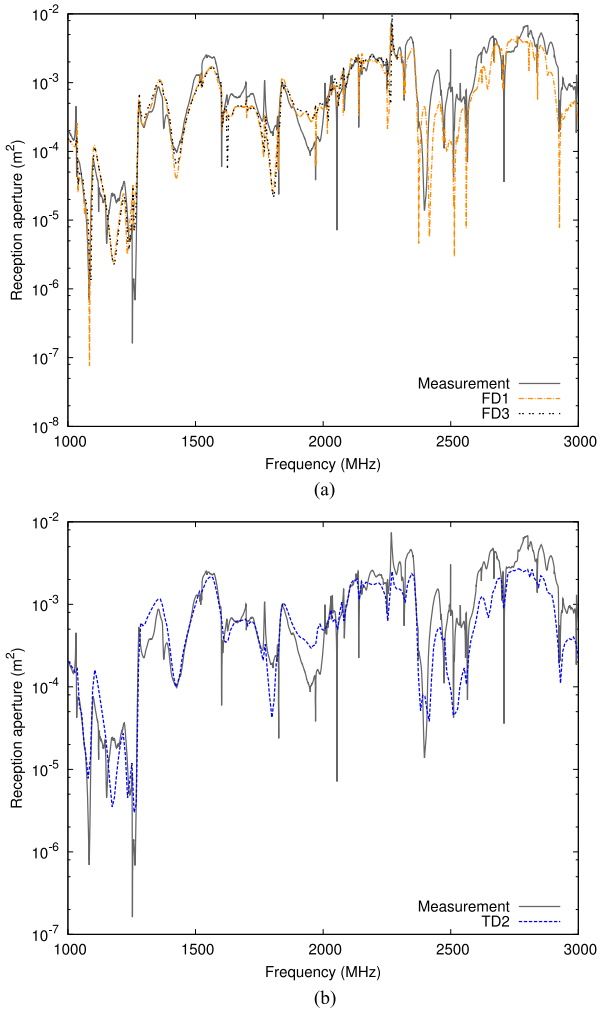

Fig. 11. Reception aperture for test-case 1 from 1–3 GHz comparing (a) frequency-domain codes and (b) time-domain codes to measurement.

files or meshes were shared between the different implementations. The results therefore intentionally reflect the variability associated with interpretation of the specification and detailed choice of modeling technique applied. We have used FSV [4] and integrated error logarithmic frequency (IELF) [22] algorithms to compare the results from the different solvers using the measurement data as a reference. The rationale is to demonstrate the variability in the results that can be expected from the implementation of a complex test-case for which analytic results are not available and choices concerning the representation of different features in the specification in a particular solver have to be made. We do not directly compare solvers (which are anonymized) with respect to their accuracy or capability, though some observations about different types of solver are made.

A. Test-Case 1

The configuration of test-case 1 consists of the enclosure with an open face and two terminated probe antennas on ports A and B. The enclosure is illuminated by a plane-wave and the power received at port A is observed. The results for two frequency-domain and one time-domain solvers are shown in Fig. 11(a) and (b), respectively. Table II shows the FSV amplitude difference measure (ADM) and feature difference measure (FDM) for each pair of results. The FSV global difference measure (GDM) and IELF values are shown in Table III.

TABLE II
FSV ADM (ABOVE DIAGONAL) AND FDM (BELOW DIAGONAL) FOR TEST-CASE 1

	Measurement	FD1	FD3	TD2
Measurement	–	**0.38**	**0.33**	**0.82**
FD1	**0.56**	–	**0.20**	**0.53**
FD3	**0.38**	**0.32**	–	**0.49**
TD2	**0.62**	**0.45**	**0.46**	–

Figures in bold correspond to quantitative FSV values less than unity.

TABLE III
FSV GDM (ABOVE DIAGONAL) AND IELF METRIC (BELOW DIAGONAL) FOR TEST-CASE 1

	Measurement	FD1	FD3	TD2
Measurement	–	**0.75**	**0.56**	1.10
FD1	0.72	–	**0.42**	**0.75**
FD3	0.56	0.21	–	**0.74**
TD2	0.73	0.50	0.34	–

Figures in bold correspond to quantitative FSV values less than unity.

Even for this simplest test-case in the test-suite, the FSV qualitative GDM is no better than "fair." IELF and the FSV GDM give consistent rankings of the data comparisons. There is no strong indication that the measurement data proves a worse reference than the solvers as a base for cross-comparisons. Overall the results seem reasonable for "one-shot" simulations with no iterative refinement of the models.

B. Test-Case 2

The second test-case is formed by adding the cube of LS22 RAM into the center of the lower surface of the enclosure and the curved wire (as shown in Fig. 3) between ports A and B to the geometry of test-case 1. The reception aperture, defined in (4), measured at port-A for this test-case is shown in Fig. 12 for two frequency-domain and three time-domain solvers. The FSV and IELF metrics are given in Tables IV and V.

For this more complex test-case, the FSV GDM is generally "poor" or "very poor" with the dominant contribution coming from the ADM. The rankings provided by IELF and FSV GDM are broadly consistent but not identical, particularly with regard to the datasets with poorer metrics. Here, there is some evidence that the measurement data provides a reference with the lowest overall metrics across all the datasets.

The measurement uncertainty itself is estimated to be no more than about 1 dB for most of the test-cases and we expect that the leading cause of the deviations is the "modeling error" introduced by the simplifications of the real physical geometry made in the simulations. The test-case is dependent on many aspects of the numerical modeling of the real system including dispersive material properties the treatment of thick wires.

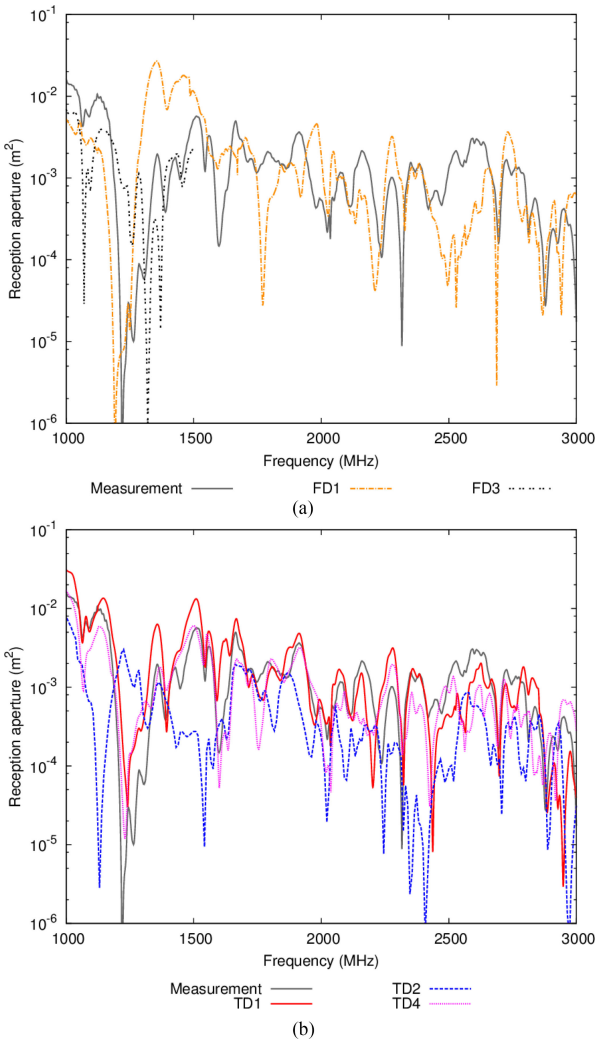

Fig. 12. Reception aperture for test-case 2 from 1–3 GHz comparing (a) frequency-domain codes and (b) time-domain codes to measurement.

TABLE IV
FSV ADM (ABOVE DIAGONAL) AND FDM (BELOW DIAGONAL) FOR TEST-CASE 2

	Measurement	FD1	FD3	TD1	TD2	TD4
Measurement	–	1.36	1.30	**0.68**	1.90	**0.48**
FD1	0.63	–	4.0	**0.75**	6.4	1.9
FD3	0.62	0.50	–	2.9	**0.99**	1.0
TD1	0.51	0.57	0.88	–	3.7	1.1
TD2	0.80	1.00	0.46	1.10	–	1.4
TD4	0.32	0.65	0.56	0.61	0.75	–

Figures in bold correspond to quantitative FSV values less than unity.

The larger spread in the FSV and IELF metrics reflects this increased complexity and highlights the need for iterative calibration of simulation tools against more realistic test-cases with multiple features.

Our purpose here was to introduce and demonstrate the test-suite; in a real-world situation further calibration of the models would be necessary if the measurement reference is assumed to be authoritative. The first step in a calibration process would be to identify dominant "modeling errors," for example, by a sensitivity analysis of the models, and then to refine the simulations accordingly until the deviation between model and measurements is comparable to the measurement uncertainty.

TABLE V
FSV GDM (ABOVE DIAGONAL) AND IELF METRIC (BELOW DIAGONAL) FOR TEST-CASE 2

	Measurement	FD1	FD3	TD1	TD2	TD4
Measurement	–	1.6	1.5	**0.92**	2.2	**0.63**
FD1	1.4	–	4.2	**1.0**	6.6	2.1
FD3	1.7	2.5	–	3.2	1.2	1.3
TD1	0.94	1.1	1.5	–	4.0	1.4
TD2	1.8	2.1	1.6	1.9	–	1.7
TD4	0.95	1.2	1.1	1.0	1.5	–

Figures in bold correspond to quantitative FSV values less than unity.

V. CONCLUSION

An extensive modular test-suite for use in VV&C of CEM solvers for EMC applications has been developed. The test-cases, while still relatively simple compared to real systems, are of a greater complexity than many of the generic canonical references currently available allowing interactions between different modeling aspects to be evaluated using a well-defined set of geometries. Hardware implementations of many of the possible test configurations have been constructed and measured to provide a database of reference data.

The test configurations have been widely used for cross-validation between different types of solvers within a number of large research programs. We have demonstrated the use of the test-suite by presenting summary results for a range of solvers applied to small subset of test-cases using the measurement data as a reference. FSV and IELF comparisons of the results highlight the difficulties inherent in the VV&C process for systems of even modest complexity and the importance of calibration to attaining reliable results.

The measurement datasets, CAD files for some of the geometries and extensions to the test-case are freely available for use [16].

ACKNOWLEDGMENT

The authors would like to thank the many contributions, in the form of corrections, clarifications of the geometries and ideas for extensions, provided by members of the HIRF-SE consortium including Jean-Philippe Parmantier of The Office National d'Etudes et de Recherches Aérospatiales (ONERA), Marco Kunze of Computer Simulation Technology (CST) AG, and John Kazik of Ingegneria dei Sistemi UK (IDS-UK). They also thank The University of Nottingham (Chris Smartt), QWED Sp.z.o.o. (Janusz Rudnicki), BAE Systems Ltd (Chris Jones and Geoff South), The Technische Universität Hamburg-Harburg (Heinz Brüns) for providing the simulations results presented in Section IV of this paper.

REFERENCES

[1] L. Sevgi, "Electromagnetic modeling and simulation: Challenges in validation, verification and calibration," *IEEE Trans. Electromagn. Compat.*, vol. 56, no. 4, pp. 750–758, Aug. 2014.

[2] W. L. Oberkampf, M. M. Sindir, and A. T. Conlisk, "Guide for the verification and validation of computational fluid dynamics simulations," Amer. Inst . Aeronaut. Astronaut., Washington, DC, USA, Report AIAA G-077-1998, 1998.

[3] O. T. Trucano and C. Hirsch, "Verification, validation and predictive capability in computational engineering and physics," *Appl. Mech. Rev.*, vol. 57, no. 5, pp. 345–384, 2004.

[4] *IEEE Standard for Validation of Computational Electromagnetics Computer Modeling and Simulations*, IEEE Standard 1597.1, 2008.

[5] *Recommended Practice for Validation of Computational Electromagnetics Computer Modeling and Simulations,* IEEE Standard P1597.2, 2010.

[6] J. F. Dawson, C. J. Smartt, I. D. Flintoft, and C. Christopoulos, "Validating a numerical electromagnetic solver in a reverberant environment," presented at the 7th Int. Conf. Computation Electromagnetics, Brighton, U.K., Apr. 2008, vol. 7–10, pp. 42–43 .

[7] C. Christopoulos *et al.*, "Characterisation and modelling of electromagnetic interactions in aircraft," *Proc. Inst. Mech. Eng., Part G, J. Aerosp. Eng.: Special Issue FLAVIIR*, vol. 224, no. 4, pp. 449–458, 2010.

[8] D. Tallini, J. F. Dawson, I. D. Flintoft, M. Kunze, and I. Munteanu, "Virtual HIRF Tests in CST STUDIO SUITE—A reverberant environment application," presented at Computational Electromagn. for Electromagn. Compat. (CEMEMC), Granada, Nevada, Spain, Sep. 12–16, 2011. pp. 849–852.

[9] J. Alvarez, L. D. Angulo, A. R. Bretones, and S. G. Garcia, "A comparison of the FDTD and LFDG methods for the estimation of HIRF transfer functions," presented at Computational Electromagn. for Electromagn. Compat. (CEMEMC), Granada, Spain, Mar. 19–21, 2013.

[10] A. C. Marvin *et al.*, "Enclosure shielding assessment using surrogate contents fabricated from radio absorbing material," in *Proc. 7th Asia-Pacific Int. Symp. Electromagn. Compat. Signal Integrity Tech. Exhib.*, Shenzhen, China, May 18–21, 2016, pp. 994–996.

[11] *Electromagnetic Compatibility (EMC) - Part 4-21: Testing and Measurement Techniques - Reverberation Chamber Test Methods*, IEC Standard 61000-4-21, 2nd ed., Jan. 2011.

[12] K. F. Casey, "Electromagnetic shielding behavior of wire-mesh screens," *IEEE Trans. Electromagn. Compat.*, vol. 30, no. 3, pp. 298–306, Aug. 1988.

[13] *Standard Test Method for Measuring the Electromagnetic Shielding Effectiveness of Planar Materials,* ASTM Standard D4935-10, Jun. 2010.

[14] C. L. Holloway, D. A. Hill, J. Ladbury, G. Koepke, and R. Garzia, "Shielding effectiveness measurements of materials using nested reverberation chambers," *IEEE Trans. Electromagn. Compat.*, vol. 45, no. 2, pp. 350–356, May 2003.

[15] I. D. Flintoft, J. F. Dawson, A. C. Marvin, and S. J. Porter, "Development of time-domain surface macro-models from material measurements," presented at the 23rd Int. Review Progress Applied Computational Electromagn., Verona, Italy, Mar. 19–23, 2007.

[16] AEG Box Test-suite, (Aug. 2016). [Online]. Available: https://bitbucket.org/uoyaeg/aegboxts

[17] Laird, "Datasheet Eccosorb LS", (Aug. 2016). [Online]. Available: http://www.eccosorb.eu/products/eccosorb

[18] B. Gustavsen and A. Semlyen, "Rational approximation of frequency domain responses by vector fitting," *IEEE Trans. Power Del.*, vol. 14, no. 3, pp. 1052–1061, Jul. 1999.

[19] C. A. Balanis, *Antenna Theory: Analysis and Design*, 3rd ed. Hoboken, NJ, USA: Wiley, 3 May 2005.

[20] Technische Universität Hamburg-Harburg. The CONCEPT-II website. (2016). [Online]. Available: http://www.tet.tuhh.de/concept

[21] T. G. Tang, Q. M. Tieng, and M. W. Gunn, "Equivalent circuit of a dipole antenna using frequency independent lumped elements," *IEEE Trans. Antennas Propag.*, vol. 41, no. 1, pp. 100–103, Jan. 1993.

[22] R. J. Simpson, C. R. Jones, I. MacDiarmid, A. Duffy, and D. Coleby, "The integrated error against log frequency (IELF) method for CEM validation," in *Proc. IEEE Int. Symp. Electromagn. Compat.*, Chicago, IL, USA, Aug. 8–12, 2005, vol. 1, pp. 296–300.

Ian D. Flintoft (M'00–SM'14) received the B.Sc. and Ph.D. degrees in physics from the University of Manchester, Manchester, U.K., in 1988 and 1994, respectively.

He is a Research Fellow in the Communication Technologies Research Group of the University of York's Department of Electronics.

John F. Dawson (M'90) received the B.Sc. and D.Phil. degrees in electronics from the University of York, York, U.K., in 1982 and 1989, respectively.

He is currently a Senior Lecturer and the Deputy Leader of the Communication Technologies Research Group at the University of York.

Linda Dawson received the B.Sc. and D.Phil. degrees in electronics from the University of York, York, U.K., in 1983 and 1990, respectively.

She is currently a Research Fellow in the Communication Technologies Research Group at the University of York.

Andrew C. Marvin (M'85–SM'06–F'11) received the B. Eng., M. Eng., and Ph.D. degrees from the University of Sheffield between 1972 and 1978. He is the Technical Director of York EMC Services Ltd and a Professor of Applied Electromagnetics in the Communication Technologies Group of the University of York's Department of Electronics.

Jesus Alvarez (M'00) received the B.Sc. degree from the University of Cantabria, Santander, Spain, in 2011 and the M.Sc. degree from the University Carlos III of Madrid in 2008, in Telecommunications Engineering, and the Ph.D. degree in Physics from the University of Granada, Spain, in 2013. Since 2006, he has been with Airbus Defence and Space, Getafe, Spain.

Salvador G. Garcia (M'93) received the M.S. and Ph.D. degrees (with extraordinary honors) in physics from the University of Granada, Granada, Spain, in 1989 and 1994, respectively.

In 1999, he joined the Department of Electromagnetism and Matter Physics, University of Granada, as an Assistant Professor (with tenure).